Journal of Colloid and Interface Science 418 (2014) 87–94

Contents lists available at ScienceDirect

Journal of Colloid and Interface Science

www.elsevier.com/locate/jcis

Au nanoplates as robust, recyclable SERS substrates for ultrasensitive chemical sensing

Wei-Hao Lin, Yi-Hsuan Lu, Yung-Jung Hsu *

Department of Materials Science and Engineering, National Chiao Tung University, Hsinchu 30010, Taiwan, Republic of China

ARTICLE INFO

Article history:
Received 1 October 2013
Accepted 29 November 2013
Available online 9 December 2013

Keywords:
Au
Nanoplates
Seed-mediated growth
Surface-enhanced Raman scattering
Single molecule detection

ABSTRACT

With the structural advantages of being sharp and straight, Au nanoplates may work as a promising surface-enhanced Raman scattering (SERS) platform for detection of Raman-sensitive analytes. However, the utilization of Au nanoplates as realistic SERS substrates is still not widely investigated, especially in the practical detection of environmentally persistent pollutants. This work delivers the first successful demonstration of using Au nanoplate platform in practical SERS sensing toward a typical polycyclic aromatic hydrocarbons pollutant of pyrene. The samples were prepared using an environmentally benign seed-mediated growth approach without the post-purification treatment. It was found that Au nanoplates exhibited significantly enhanced SERS activities (enhancement factor = 7.30×10^7) and achieved an extremely low detection limit (5×10^{-10} M) toward pyrene molecules. Furthermore, the SERS activity of Au nanoplates can be fully recovered after repeatedly used and recycled in pyrene detection. These results manifest that the present Au nanoplates can serve as robust, recyclable SERS substrates that allow rapid detection of trace levels of analytes with a high degree of sensitivity and stability. The findings from this work may facilitate the use of Au nanoplate SERS substrates in more realistic applications such as biomolecule sensing and environmental monitoring.

1. Introduction

Over the past decade, surface-enhanced Raman scattering (SERS)-based chemical sensors have been extensively explored because million-fold enhancement in detection sensitivity can be acquired [1]. When molecules are deposited on rough noble metal surfaces, they show greatly enhanced Raman scattering, which is known as SERS effect and is a useful means to gain chemical information for molecules adsorbed on metal surfaces. The enhancement of SERS signals can be attributed to two effects, the electromagnetic (EM) effect and the chemical enhancement mechanism. The EM effect describes the enhanced electromagnetic field induced by the surface plasmon resonance (SPR) excitation of metal substrate, which magnifies incident light intensity to increase the signals of Raman scattering. The chemical enhancement mechanism states the charge transfer between metal surfaces and adsorbed molecules, which results in an increased polarizability of the molecules and thus the signal amplification of Raman scattering. It is generally believed that EM is the main contribution for signal enhancement when using noble metal nanocrystals as SERS substrates. Besides, theoretical calculations suggest that electromagnetic field is enhanced by several orders at the sharp corners and fractal edges of metal surfaces [2], thereby making anisotropic nanocrystals excellent candidates for SERS substrates. Until now, many anisotropic metal nanostructures including nanowires [3,4], nanoplates [5–8], nanoflowers [9–11], polyhedral nanocrystals [12,13], and other hierarchical nanoarchitectures [14–19] have been proven effective in the detection of Raman-sensitive analytes.

Among the various anisotropic nanocrystals of Au, nanoplates may work as a promising SERS platform since the sharp corners and straight edges are supposed to induce significantly enhanced electromagnetic field [20–25]. Although the optical properties of Au nanoplates have been well studied, their utilization as realistic SERS substrates is still not widely investigated, especially in the practical detection of environmentally persistent pollutants. Quite many approaches for the preparation of Au nanoplates have been developed and reported in the literatures [20–41]. Most of them involve the post-purification treatment [26–29], the prolonged aging time [30,31], or the use of environmentally harmful chemicals [22–35], which are relatively elaborate and may hinder the applicability of the products. In this work, a facile, environmentally benign seed-mediated growth approach was developed to obtain Au nanoplates in high yield. We systematically investigated the growth mechanism of the Au nanoplates, interpreted the SPR absorption features of the samples, quantitatively evaluated the SERS activities of the samples, and most importantly demonstrated the realistic and remarkable SERS applications of Au nanoplates in

* Corresponding author. Fax: +886 35724727.
E-mail address: yhsu@cc.nctu.edu.tw (Y.-J. Hsu).

0021-9797/$ - see front matter © 2013 Elsevier Inc. All rights reserved.
http://dx.doi.org/10.1016/j.jcis.2013.11.082

polycyclic aromatic hydrocarbons detection. In contrast to most of the previously reported methods to achieve high yield production of Au nanoplates, cetyltrimethylammonium bromide (CTAB), which is regarded as highly cytotoxic, was not required in the current method. The success of the method relied on the employment of defect-existing Au particle seeds which induced and directed the two-dimensional anisotropic growth of nanoplates. The synthesis used water-soluble, physiologically compatible poly(N-vinylpyrrolidone) (PVP) as reducing agent and capping reagent, and was accomplished at room temperature in 4 h without the post-purification treatment. Since the nucleation and growth stages are separated in the seed-mediated growth process, a better control over the shape uniformity for the products can be acquired [42]. By suitably modulating the molar ratio of PVP to $HAuCl_4$ used in the growth process, a controllable yield of nanoplates in the products can be achieved, from 32.0% to 96.8%. With this outcome, we were able to study the morphology effect of Au on the resultant SERS performance. The SERS properties of the samples with different nanoplate yields were investigated by using two representative Raman-sensitive analytes, MB and pyrene, as the probe molecules. The SERS enhancement factor of nanoplate-dominant sample (nanoplate yield = 96.8%) for the adsorbed MB molecules was 7.30×10^7, exceeding twenty times the value obtained by nanoparticle-enriched sample (nanoplate yield = 32.0%). The SERS efficiency of nanoplate-dominant sample was further examined in the practical detection of pyrene, a typical polycyclic aromatic hydrocarbon pollutant that is commonly distributed in the environment. The nanoplate-dominant sample achieved a remarkable detection limit of 5×10^{-10} M toward pyrene molecules, demonstrating the capability of single molecule detection for Au nanoplates. Furthermore, the SERS activity of nanoplate-dominant sample can be fully recovered after repeatedly used and recycled in pyrene detection. These results manifest that the present Au nanoplates can serve as robust, recyclable SERS substrates that allow rapid detection of trace levels of analytes with a high degree of sensitivity and stability.

2. Experimental details

2.1. Chemicals

All chemicals including tetrachloroauric acid ($HAuCl_4$), poly(N-vinylpyrrolidone) (denoted as PVP, M_W = 10,000 or 29,000 Da), methylene blue ($C_{16}H_{18}N_3SCl$, denoted as MB), lucigenin ($C_{28}H_{22}N_4O_6$), and pyrene ($C_{16}H_{10}$) were of analytical grade and used without further purification.

2.2. Synthesis of Au nanoplates

The samples were prepared using a seed-mediated growth approach described in our previous work with slight modifications [43]. Two stock solutions of PVP were prepared in advance and were denoted as PVP-1 (M_w = 10,000 Da, 0.01 M) and PVP-2 (M_w = 29,000 Da, 0.01 M). In the typical procedure, PVP-1 (8 mL) and $HAuCl_4$ aqueous solution (0.065 mL, 0.01 M) were first mixed in a stainless-steel vial with a capacity of 20 mL and then diluted to a total volume of 10 mL using deionized water. After being sealed, the vial was heated at 130 °C in oil bath to produce Au seed particles with an average size of 6.0 nm. To obtain Au nanoplates, Au seed solution (0.1 mL) and PVP-2 (10 mL) were mixed in a glass vial, followed by the addition of $HAuCl_4$ aqueous solution (1 mM, 9.9 mL). The mixed solution was then aged at 25 °C for 4 h to result in the formation of Au nanoplates. The product was collected by centrifugation and washed with acetone and ethanol to remove excess PVP. In this work, four various molar ratios of PVP to $HAuCl_4$ (40, 20, 10, 5) were used in the later growth process to produce samples with different nanoplate yields. Note that PVP-2 which has longer alkyl chain than PVP-1 was suggested to exhibit lower reducing power when employed in the growth stage [39]. Such a substantially low reducing power of PVP-2 is instrumental in promoting the kinetic control mode for crystal growth, which conduces to the formation of nanoplates with high morphological yield. It should be mentioned that if PVP-1 was continuously used in the growth stage, a fairly mediocre nanoplate yield may result, revealing the indispensability of adequate PVP to the high-yield production of the present Au nanoplates.

2.3. Preparation of SERS substrates

SERS substrates were prepared by dripping sample suspensions with a fixed amount on a 0.3 cm × 0.3 cm Si wafer. This procedure has been widely used and proven valid for SERS substrate preparation [5,9,10,18–21,25]. After completely dried, the substrate was heated at 200 °C for 3 h to remove the PVP covered on the surfaces of Au, which was confirmed by the significantly depressed C=O band recorded in the Fourier transform infrared (FTIR) absorption spectrum (data not shown). Note that no noticeable change in morphology can be found for the sample deposited on Si wafer upon the heat treatment. The thus-obtained substrate was immersed in MB aqueous solution (10^{-5} M) for 1 h. The substrate was then taken out, rinsed with deionized water to remove any un-adsorbed MB molecules, and dried at 60 °C for later use. It has been demonstrated that the electromagnetic field of SPR decreases with increasing distance from the metal surface [2]. If heat treatment was not taken on the sample, the existed PVP would increase the distance between the MB molecules and the Au surface, giving rise to a weakened electromagnetic field for MB and thus a depressed SERS intensity. To probe pyrene molecules, the heat-treated substrate containing a fixed amount of nanoplate-dominant sample was immersed in lucigenin aqueous solution (10^{-3} M) to functionalize the surface of Au. Afterward, aqueous solutions of pyrene (10 μL) with different concentrations were dropped on the substrate surface. The substrate was then dried in air for later spectroscopy measurement.

2.4. Characterizations

The morphology and dimensions of the samples were examined with a field-emission scanning electron microscope (SEM, Jeol, JSM-6500F) and a high-resolution transmission electron microscope (HRTEM, Jeol, JEM-2100) operated at 200 kV. The morphological yield of nanoplates for the samples was determined by examining hundreds of nanocrystals from the low-magnification TEM images. The relative volume proportions were then calculated and represented. The thickness of individual nanoplate was measured by using an atomic force microscope (AFM, Veeco, Escope) in tapping mode. The crystallographic structure of the samples was investigated with powder X-ray diffraction (XRD, Bruker, D2 phaser), HRTEM, and selected-area electron diffraction (SAED, an accessory of the HRTEM). UV–visible–NIR extinction spectra were obtained from a Jasco V-670 spectrophotometer at room temperature. SERS measurements were performed by a Horiba Jobin Yvon HR800 microscopy Raman spectroscope equipped with a liquid nitrogen-cooled charge-coupled device detector. The SERS excitation wavelength was 632.8 nm provided by the He—Ne laser with a power of 20 mW. To collect the Raman spectrum of MB solution, a 50× objective with a numerical aperture of 0.55 was applied. During the SERS measurement, a 100× objective with a numerical aperture of 0.9 was used, which gives a laser spot size of 0.857 μm. Besides, the acquisition time was set as 12 s for each spectrum, and all the spectra were calibrated using 520 cm^{-1} band of Si wafer. It

should be noted that the variation of Raman intensity recorded from different regions of the samples was less than 10%, indicating good homogeneity of the samples deposited on the substrate and high reproducibility of the resultant SERS performance.

3. Results and discussion

3.1. Structural investigation

First, Au nanoparticles with an average size of 6.0 nm and a size distribution of 6.5% were obtained using the PVP-assisted hydrothermal method. HRTEM characterization in Fig. 1 shows that the as-prepared Au nanoparticles were crystalline with apparent structural defects of twin boundaries. The Au nanoparticles were then used as the seeds for the subsequent growth of Au nanoplates. PVP was used as both reducing agent and capping reagent in the later growth process. In this work, four various molar ratios of PVP to $HAuCl_4$ ($R_{PVP/Au}$) were employed to obtain products with different nanoplate yields, with which the morphology effect of Au on the resultant SERS performance can be studied. SEM observations reveal that the four products all consisted of a mixture of platelet-like nanostructures and pseudo-spherical nanoparticles differing in the morphological yield. As shown in Fig. 2, the nanoplates, which were triangular, truncated triangle and hexagonal in geometry, had a typical edge length of 50–500 nm, while the size of pseudo-spherical particles was in the range of 30–100 nm. The sample obtained with $R_{PVP/Au}$ of 40 was mainly composed of polyhedral nanoparticles and had a fairly low nanoplate yield of 32.0%. As decreasing $R_{PVP/Au}$ to 20, platelet structures with a yield of 40.3% were found prevalent in the product. When $R_{PVP/Au}$ was lowered to 10, nanoplates became the dominant product instead of nanoparticles, corresponding to a drastically increased yield of 96.8%. A reduced yield of 55.8% for the grown nanoplates was however observed if $R_{PVP/Au}$ was further decreased to 5. This outcome implies that there was an optimal $R_{PVP/Au}$ for obtaining Au nanoplates in high yield by using the seed-mediate growth method. Further structural investigation was carried out using XRD. Fig. S1 (Supporting material) shows the corresponding XRD patterns for the four samples. All the diffraction peaks can be indexed to face-centered cubic (*fcc*) Au. In addition, a relatively intense (111) peak as compared to the standard pattern was recorded, with nanoplate-dominant sample ($R_{PVP/Au}$ = 10) showing the lowest intensity ratio of (200) to (111), as was clearly noted in Table 1. This phenomenon implies that {111} facets comprised the top and bottom surfaces of Au nanoplates [36–40], which can be further confirmed by HRTEM and SAED analyses.

To learn more information about the as-obtained Au nanoplates, TEM, AFM, HRTEM, and SAED measurements were conducted. Fig. 3(a) shows the typical TEM image of nanoplate-dominant sample. Evident contrast variations arising from the structural bending and uneven stresses were observed across the nanoplate surface, which is characteristic of thin nanostructures. AFM characterization was performed to delineate the shape and dimension of Au nanoplates. As revealed in the inset of Fig. 3(a), the obtained Au nanoplates had considerably smooth surface and were of about 20 nm in thickness. Fig. 3(b) presents the HRTEM image taken on an individual hexagonal nanoplate. The lattice image clearly reveals the {−220} lattice planes of *fcc* Au with the *d* spacing of about 0.14 nm. As indicated by the inset arrows in Fig. 3(b), the growth directions along the six corners of the nanoplates can be indexed as six equivalent {−110} directions. The corresponding SAED pattern of Fig. 3(c) suggests the single-crystalline nature of the nanoplate product. The diffraction spots with 6-fold rotational symmetry result from the projection of *fcc* Au along the [111] zone axis, manifesting that the top and bottom faces of Au nanoplates were enclosed by {111} planes. Besides, the formally forbidden reflections of 1/3{−422} and 2/3{−422} which are typically found in platelet nanostructures were also recorded [44,45]. The existence of dislocations or stacking faults parallel to the {111} surfaces of nanoplates may be responsible for the appearance of such forbidden reflections. As depicted in Fig. 3(d), a dislocation on (111) plane of *fcc* Au with burgers vector of a/2[10−1] can decompose into two partial dislocations of a/6[2−1−1] and a/6[11−2] in order to minimize the total energy [46]. Dislocation via this two-step process creates a stacking fault in a new stacking sequence of AB|ABCA, where | represents the location of stacking fault. In such ABABCA stacking, there exist four planes with the stacking of ABAB, which is exactly the stacking sequence of hexagonal close-packed (*hcp*) structure along [001]. The derived diffraction planes of $\{100\}_{hcp}$ have lattice spacing (0.25 nm) exactly equal to the spacing of 1/3{−422} of the primary *fcc* Au. Therefore, diffraction spots which essentially represent $\{100\}_{hcp}$ reflections were noted as 1/3{−422} in the SAED of Au nanoplates. According to XRD and SAED data, we suggested that Au nanoplates were grown along the preferential growth direction perpendicular to the normal direction of the two {111} basal surfaces, which is {−110} as judged from HRTEM analysis.

3.2. Growth mechanism

There have been numerous synthetic approaches developed for preparation of novel metal nanoplates [5–8,20–41,45]. Based on the experimental conditions and results, many plausible growth mechanisms for the formation of nanoplates were proposed and examined. The common feature is the sufficiently slow reaction rate which triggers the kinetic control regime for crystal growth

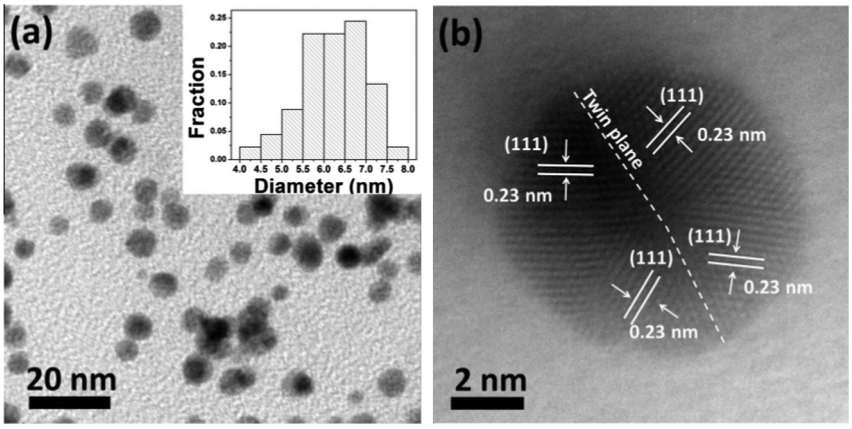

Fig. 1. (a) TEM and (b) HRTEM image of Au particle seeds.

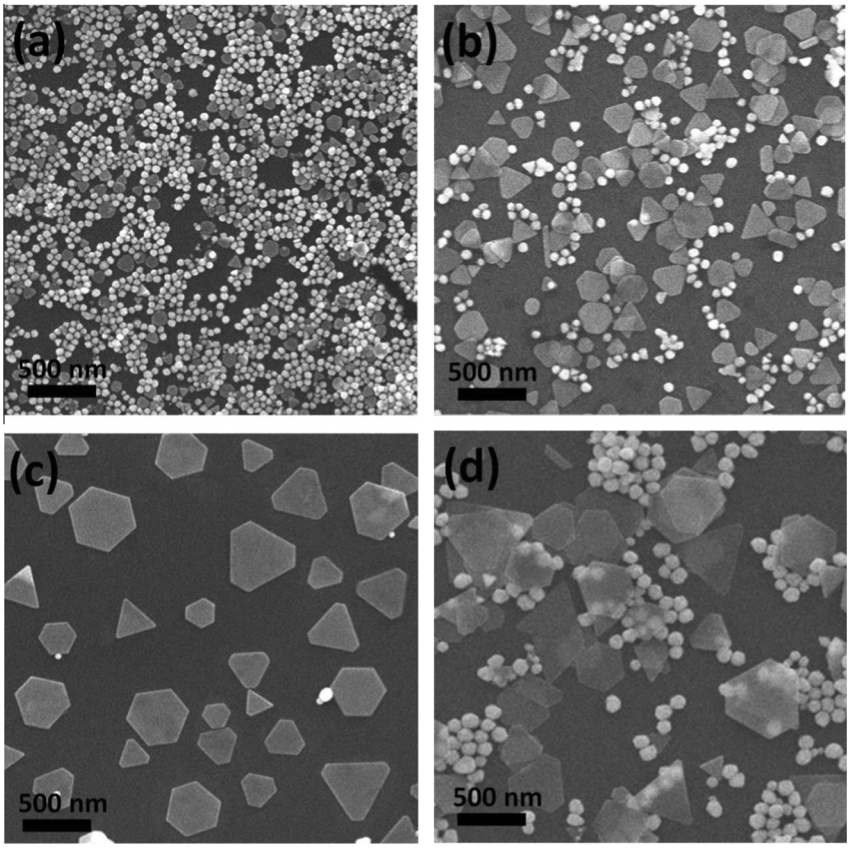

Fig. 2. SEM images of the samples prepared with $R_{PVP/Au}$ of (a) 40, (b) 20, (c) 10, and (d) 5.

Table 1
The morphological yield, XRD intensity ratio of (200) to (111), and *EF* value of the samples prepared with different $R_{PVP/Au}$ values.

$R_{PVP/Au}$	Nanoplate yield (%)	$I_{(200)}/I_{(111)}$ of XRD[a]	*EF* of SERS
40	32.0	0.055	0.33×10^7
20	40.3	0.040	1.07×10^7
10	96.8	0.014	7.30×10^7
5	55.8	0.028	1.25×10^7

[a] The $I_{(200)}/I_{(111)}$ value of bulk reference Au (JCPDS 89-3697) is 0.52.

to render the formation of such thermodynamically unfavorable shape. In the current reaction system, Au particle seeds with structural defects were employed to induce and direct the two-dimensional anisotropic growth of nanoplates. It is an established fact that the final shape of nanocrystals is determined by not only the growth rates of different crystallographic facets but also the crystallinity of seed nuclei [47]. In this work, PVP may substantially slow down the hydrothermal reaction rate to produce Au particle seeds with structural defects thanks to its weak reducing power. As displayed in Fig. 1, TEM analysis demonstrates that the as-prepared Au seed particles were characterized by apparent planar defects like twin planes. These defect-existing seeds can further evolve to possess edges which were essentially unstable and thus inclined to be attached by the feed atoms [48]. At the same time, PVP which selectively bound to {1 1 1} facets of Au [36] would expedite preferential growth along the lateral directions of {−1 1 0}, leading to two-dimensional anisotropic growth to cause nanoplate formation. Consistent with this supposition is the geometry model of Au nanoplates derived from XRD, HRTEM, and SAED analyses. In an ideal situation, crystal growth of Au along the six equivalent {−1 1 0} directions at the two-dimensional basal plane was prevalent, resulting in the formation of hexagonal nanoplates enclosed by alternate lateral faces of {1 0 0} and {1 1 1} [6,49]. However, because of the inevitable temperature fluctuation during the reaction process, nonequivalent growth among the six {−1 1 0} directions may take place, leading to the possible appearance of triangular and truncated triangle structures in the product [50]. It is important to remark that without the presence of seeds in the growth solution, only irregularly shaped nanocrystals were obtained, implying that the pre-synthesized defect-existing seeds are an indispensable initiator for the kinetically controlled synthesis of Au nanoplates. In addition to the employment of defect-existing Au seeds, the molar ratio of PVP to $HAuCl_4$ used in the later growth process is also crucial. It has been reported that the reaction kinetics of metal nanocrystal synthesis can be delicately manipulated by controlling the molar ratio of PVP to metal precursor [36–38]. Under a high PVP/$HAuCl_4$ ratio condition ($R_{PVP/Au}$ = 40, 20), $AuCl^{4-}$ ions were reduced sufficiently rapidly due to the increasing reducing power of the relatively abundant PVP. The fast reduction rate may trigger the thermodynamically controlled regime for crystal growth, resulting in the formation and prevalence of polyhedral nanoparticles [38]. On the other hand, the growth of nanoplates was restrained in the situation of low PVP/$HAuCl_4$ ratio ($R_{PVP/Au}$ = 5) because PVP with insufficient amount cannot effectively cover {1 1 1} facets of Au to expedite two-dimensional anisotropic growth. As a result, more isotropic and even irregularly shaped nanocrystals became significantly popular in the product.

3.3. SPR absorption and SERS properties

With the inherently prominent anisotropic structures, Au nanoplates are expected to display unique SPR features. Fig. S2 (Supporting material) represents the UV–visible–NIR extinction

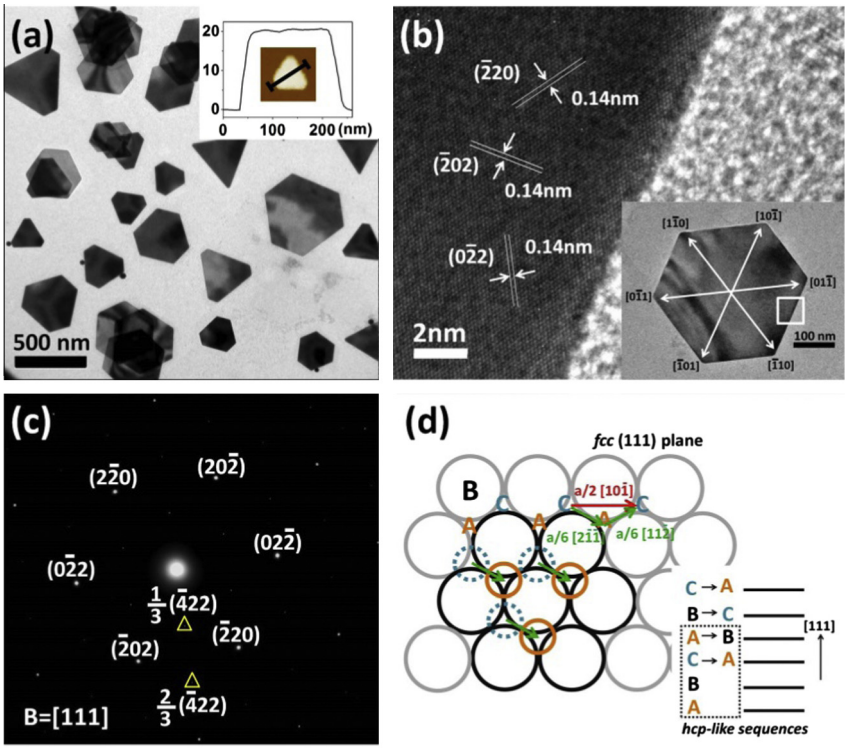

Fig. 3. Au nanoplates from nanoplate-dominant sample: (a) TEM image and AFM analysis (inset), (b) HRTEM image, (c) SAED pattern, and (d) schematic illustration for the appearance of forbidden reflections in (c).

spectra taken from the aqueous suspensions of the four products. For the sample prepared with $R_{PVP/Au} = 40$ (nanoparticle-enriched sample), a predominant absorption peak positioned at 585 nm was observed, attributable to the SPR absorption of the constituent polyhedral nanoparticles [51]. The sample obtained from $R_{PVP/Au} = 20$ was however characterized by two SPR absorptions. The first absorption, located at 585 nm, mainly originated from the polyhedral nanoparticles that existed in the product. The second absorption, centered at 924 nm, was ascribed to the grown nanoplates with the edge length of 100–150 nm [20]. Note that due to the significant surface polarization at the sharp corners, nanoplates showed SPR absorption that was red-shifted from the more isotropic polyhedral nanoparticles [52]. For the sample prepared with $R_{PVP/Au} = 10$ (nanoplate-dominant sample), an absorption band spanning from visible to near-infrared region was recorded. This band, centered around 1300 nm, was significantly red-shifted as compared to the nanoplate-related SPR peak observed in the sample with $R_{PVP/Au} = 20$. The increased charge separation resulting from the prolonged edge length of the composing nanoplates (200–500 nm) conduces to the significant red-shift in SPR absorption [52,53]. It should be noted that no definite absorption peak around 585 nm can be recognized in the spectrum of nanoplate-dominant sample, implying that the sample was almost purely composed of nanoplates as consistent with the high nanoplate yield of 96.8%. As to the sample obtained from $R_{PVP/Au} = 5$, a major absorption band at 1023 nm accompanied with a slight shoulder at 570 nm was measured. These two SPR absorptions were respectively assigned to nanoplates and isotropic nanocrystals present in the product.

The large anisotropy of Au nanoplates should substantially influence the resultant SERS properties. In particular, the sharp corners and straight edges of nanoplates can produce more hot spots for enhancing Raman scattering of the adsorbed molecules. In this work, MB, an organic dye showing no fluorescence interference with its Raman signal [54], was chosen as the probe molecule to quantitatively evaluate the SERS activity of the sample. For SERS spectroscopy, the highest EM field enhancement is attained when the irradiation wavelength is resonant with SPR maximum of the metal. As illustrated in Fig. S2, the nanoplate-dominant sample exhibited a broad SPR absorption band centered around 1300 nm, while the nanoparticle-enriched sample had a predominant SPR peak positioned at 585 nm. To stress the superior SERS activity of Au nanoplates over more isotropic pseudo-spherical nanoparticles, we used a 632.8 nm excitation laser which interacts moderately with nanoplates but intensely with nanoparticles to perform the measurement. Fig. S3 (Supporting material) compares the SERS spectra of MB adsorbed on substrates containing the four different samples. The primary characteristic peaks at 1625, 1396, and 450 cm^{-1} were related to the adsorbed MB molecules and can be assigned to C—C ring stretching, C—N symmetric stretching, and C—N—C skeletal bending modes, respectively [55]. As evident from Fig. S3, all the four samples displayed well-resolved SERS spectra, with nanoplate-dominant one showing the strongest enhancement. This outcome demonstrates that Au nanoplates are especially active for SERS detection of molecular species, which is most likely related to their sharp corners and straight edges. To quantify the result of Fig. S3, we calculated the enhancement factor (*EF*) using the following expression [7,9,56]

$$EF = \frac{I_{SERS}/N_{SERS}}{I_{Bulk}/N_{Bulk}},$$

where I_{SERS} and I_{bulk} are the integrated intensities of a chosen band (1625 cm^{-1}) for the adsorbed and unadsorbed MB molecules, respectively, and N_{SERS} and N_{bulk} correspond to the numbers of MB which contribute to the signals.

A series of evaluation steps were then performed to approximate the values of N_{bulk} and N_{SERS} for different samples (see Supporting material). Computing I_{SERS} and I_{bulk} at 1625 cm^{-1}, we obtained *EF* as 0.33×10^7, 1.07×10^7, 7.30×10^7, and 1.25×10^7 for the sample with $R_{PVP/Au}$ of 40, 20, 10, and 5. It was found that the *EF* of the sample increased with increasing nanoplate yield.

This result can be rationalized by the fact that more vigorous SERS activity was attained from sample with higher nanoplate yield, which possessed more sharp corners and straight edges acting as SERS hot spots. Furthermore, in comparison with nanoparticle-enriched sample ($R_{PVP/Au}$ = 40), nanoplate-dominant sample ($R_{PVP/Au}$ = 10) exhibited twenty times higher activity for the SERS detection of MB molecules. This demonstration addresses the benefit of the two-dimensionally anisotropic nanoplates for SERS applications. It should be noted that although triangular and hexagonal shapes were simultaneously existent in the nanoplate-dominant sample, their contribution to SERS enhancement was suggested to be nearly significant considering that they both possessed the structural advantages of being sharp and straight.

3.4. Practical SERS sensing toward pyrene molecules

To further explore the potential as a reliable SERS platform for Au nanoplates, the performance of nanoplate-dominant sample in the detection of polycyclic aromatic hydrocarbons (PAHs) was evaluated. PAHs are ubiquitous environmental pollutants originating from the incomplete combustion of organic matters such as petroleum. Being potentially carcinogenic to humans, PAHs are of great concern and the detection of them at trace concentrations has been imperative. Identification of PAHs is usually carried out by liquid chromatography with UV–visible and fluorescence detectors or gas chromatography with mass spectrometry [57], which is elaborate, time-consuming, and thus unsuitable for routine analysis. The significant SERS effect of Au nanoplates may provide an alternative for detecting PAHs in a more efficient, handy manner. Here, we chose pyrene as the testing model of PAHs because of its simple structure. Since pyrene shows relatively low affinity to metals, it is necessary to chemically modify the surface of Au to afford facile connection between them. Lucigenin, typically used for functionalization of metal electrodes, has been employed as the bifunctional linker to couple Ag nanoparticles with aromatic organic pollutants, which renders efficient SERS sensing for pollutant molecules [58,59]. In this experiment, lucigenin was used as the molecular linker to facilitate the approach of pyrene to the surface of Au. As represented in Fig. 4, several additional SERS peaks were observed for nanoplate-dominant sample upon the surface modification with lucigenin. These distinctive peaks, mainly located at 1394, 1266, and 1034 cm^{-1}, were respectively attributed to the C—C in-plane stretching, C—C inter-ring stretching, and in-plane ring breathing of the attached lucigenin [59]. The relatively intense peak at 1394 cm^{-1} suggests that lucigenin was bound onto the sample surface, probably through the formation of Au—N bonds, with its backbone perpendicular to Au surface [59]. The acridinium groups of lucigenin which faced outward from sample surface can then form intermolecular cavities to host the target pyrene molecules. As can be seen in Fig. 4, after the introduction of a trace amount of pyrene (10^{-4} M), the lucigenin-modified sample exhibited recognizable SERS signals associated with pyrene molecules, mainly located at 1246 (C—H bending), 1404 (C—C aromatic ring stretching), and 1586 cm^{-1} (C—C stretching). This phenomenon manifests that pyrene molecules were successfully recognized on Au nanoplate SERS substrate. Additionally, an evident shift toward higher frequency was observed for all the lucigenin related vibrations, which is a consequence of the effective interaction between lucigenin and pyrene [60]. The *EF* value of pyrene was also estimated from the spectral comparison between the bulk reference (pyrene powder) and the adsorbed pyrene on Au nanoplates. As shown in Fig. S5 (Supporting material), a quantitative comparison of the integrated intensity at 1404 cm^{-1} between the bulk reference (I_{bulk} = 212 for 10^{-2} M pyrene) and the adsorbed pyrene (I_{SERS} = 19,798 for 10^{-6} M pyrene) gave an apparent *EF* value of 0.93×10^6. Note that the exact *EF* value of pyrene should have been significantly larger and comparable to the value of MB, considering that Au nanoplates were not distributed on the whole substrate surface, and therefore, the practical number of pyrene probed was essentially lower.

To test the applicability of Au nanoplate SERS platform in a more realistic sensing system, the limit of detection toward pyrene molecules was evaluated. Fig. 5 shows the SERS responses of the lucigenin-modified nanoplate-dominant sample upon the addition of pyrene at seven decreasing concentrations. The C—C aromatic ring stretching band at 1404 cm^{-1} was chosen as the representative signal for recognition of the target pyrene. As noticed in Fig. 5, nanoplate-dominant sample exhibited very low detection limit toward pyrene molecules. Even when the pyrene concentration was decreased to 10^{-10} M, the Raman signal at 1404 cm^{-1}

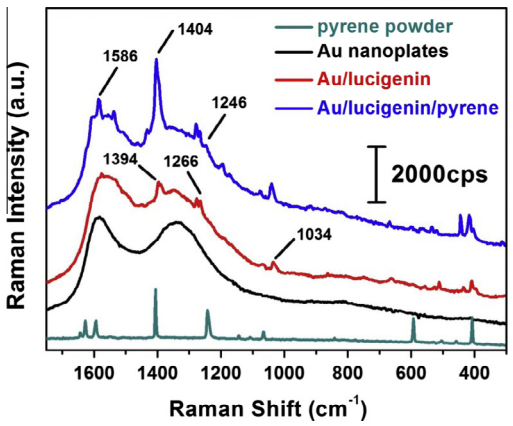

Fig. 4. SERS spectrum of pyrene molecules (10^{-4} M) adsorbed on substrate containing the lucigenin-modified nanoplate-dominant sample. The Raman spectra of pyrene powder, non-modified nanoplate-dominant sample, and lucigenin-modified nanoplate-dominant sample were also included for comparison.

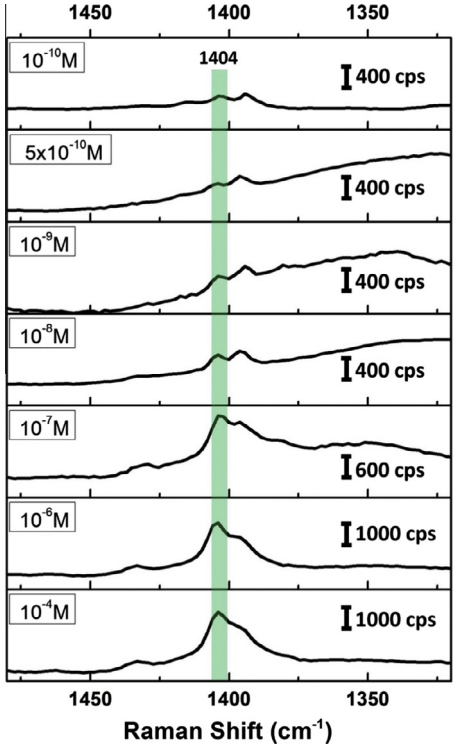

Fig. 5. SERS responses of the lucigenin-modified nanoplate-dominant sample upon the addition of pyrene at seven decreasing concentrations.

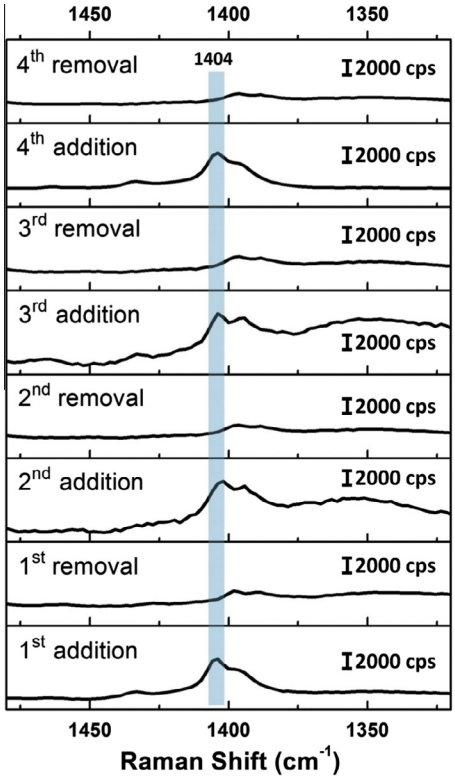

Fig. 6. SERS responses of the lucigenin-modified nanoplate-dominant sample during four repeating cycles of pyrene detection.

was still distinguishable. By examining the signal with a reasonable resolution of S/N ratio of 10 [61], the limit of detection of nanoplate-dominant sample toward pyrene molecules was estimated to be 5×10^{-10} M, which is much lower than some previously reported values of Ag nanoparticle SERS substrates ($10^{-8} \sim 10^{-9}$ M) [58,59,62,63]. We attributed this superiority to the structural feature of Au nanoplates which induced significant enhancement of local electromagnetic field to promote the resultant SERS. It should be mentioned that a much stronger SERS activity can be acquired if an appropriate excitation laser which interacts more intensely with the SPR maximum of Au nanoplates is used. The exceptional chemical sensitivity of Au nanoplates should make them especially useful for SERS-based single molecule detection. To further demonstrate the robustness of the Au nanoplate SERS substrate, we examined the recyclable application by performing repeating cycles of pyrene detection. In each cycle of the detection, the Au nanoplate substrate with pyrene attached was first characterized with Raman spectroscopy, followed by a thorough rinsing with methanol to remove the hosted pyrene molecules. Here, methanol was used to remove pyrene molecules from substrate surface by virtue of its relatively good solvation ability toward pyrene. Upon the rinsing treatment, the main band of pyrene (at 1404 cm^{-1}) lost its intensity, and the Raman spectrum of the substrate resembled that of the fresh lucigenin-modified substrate. After the Au nanoplate substrate became clean, it can be used to host pyrene molecules for the second run of detection. It is important to note that the substantial Au—N bonds formed between Au and lucigenin enabled the preservation of acridinium moieties at substrate surface during the rinsing process, through which the attachment of pyrene molecules may proceed in the subsequent detection runs. As shown in Fig. 6, after repeatedly used and recycled in pyrene detection for four cycles, the efficiency of the substrate was almost fully maintained, revealing the feasibility as a recyclable SERS substrate for the present Au nanoplates.

4. Conclusions

In conclusion, a facile seed-mediated growth approach was developed to prepare Au nanoplates in high yield without the post-purification treatment or the use of highly toxic chemicals such as CTAB. By suitably modulating the molar ratio of PVP to $HAuCl_4$ employed in the growth process, a controllable yield of nanoplates in the products can be achieved, from 32.0% to 96.8%. The success of the approach relied on the employment of defect-existing Au particle seeds which induced and directed the two-dimensional anisotropic growth of nanoplates. With the structural advantages of being sharp and straight, Au nanoplates exhibited significantly enhanced SERS activities with an enhancement factor of 7.30×10^7. The SERS efficiency of Au nanoplates was further examined in the practical detection of pyrene molecules, which achieved a remarkable detection limit of 5×10^{-10} M. Moreover, recycling test reveals that Au nanoplates can be reused multiple times in SERS detection without significant loss of the activity. The biocompatible Au nanoplates with such superior SERS properties may open new avenues for unique applications in biomolecule sensing and environmental monitoring where the detection and identification of targets at single molecule level are essential. The ability to synthesize Au nanoplates in large scale by using reproducible seed-mediated approach may inspire more diverse applications for Au nanoplates.

Acknowledgment

This work was financially supported by the National Science Council of Republic of China (Taiwan) under Grant NSC-100-2113-M-009-004.

Appendix A. Supplementary material

Supplementary data associated with this article can be found, in the online version, at http://dx.doi.org/10.1016/j.jcis.2013.11.082.

References

[1] R.A. Alvarez-Puebla, L.M. Liz-Marzán, Chem. Soc. Rev. 41 (2012) 43–51.
[2] K.L. Kelly, E. Coronado, L.L. Zhao, G.C. Schatz, J. Phys. Chem. B 107 (2003) 668–677.
[3] S. Preciado-Flores, D.A. Wheeler, T.M. Tran, Z. Tanaka, C. Jiang, M. Barboza-Flores, F. Qian, Y. Li, B. Chen, J.Z. Zhang, Chem. Commun. 47 (2011) 4129–4131.
[4] R.A. Alvarez-Pueblaa, E.R. Zubarevb, N.A. Kotovc, L.M. Liz-Marzán, Nano Today 7 (2012) 6–9.
[5] Y. Xiong, J.M. McLellan, J. Chen, Y. Yin, Z.-Y. Li, Z. Xia, J. Am. Chem. Soc. 127 (2005) 17118–17127.
[6] Y. Yang, S. Matsubara, L. Xiong, T. Hayakawa, M. Nogami, J. Phys. Chem. C 111 (2007) 9095–9104.
[7] Y. Wang, X. Zou, W. Ren, W. Wang, W. Wang, J. Phys. Chem. C 111 (2007) 3259–3265.
[8] D. Jana, A. Mandal, G. De, ACS Appl. Mater. Interfaces 4 (2012) 3330–3334.
[9] B.K. Jena, B.K. Mishra, S. Bohidar, J. Phys. Chem. C 113 (2009) 14753–14758.
[10] T. Liu, D. Li, D. Yang, M. Jiang, Langmuir 27 (2011) 6211–6217.
[11] H.M. Song, L. Deng, N.M. Khash, Nanoscale 5 (2013) 4321–4329.
[12] Z. Zhu, H. Meng, W. Liu, X. Liu, J. Gong, X. Qiu, L. Jiang, D. Wang, Z. Tang, Angew. Chem. Int. Ed. 50 (2011) 1593–1596.
[13] H.-L. Wu, H.-R. Tsai, Y.-T. Hung, K.-U. Lao, C.-W. Liao, P.-J. Chung, J.-S. Huang, I.-C. Chen, M.H. Huang, Inorg. Chem. 50 (2011) 8106–8111.
[14] P. Xu, B. Zhang, N.H. Mack, S.K. Doorn, X. Han, H.-L. Wang, J. Mater. Chem. 20 (2010) 7222–7226.
[15] P. Xu, N.H. Mack, S.-H. Jeon, S.K. Doorn, X. Han, H.-L. Wang, Langmuir 26 (2010) 8882–8886.
[16] B. Zhang, P. Xu, X. Xie, H. Wei, Z. Li, N.H. Mack, X. Han, H. Xu, H.-L. Wang, J. Mater. Chem. 21 (2011) 2495–2501.
[17] S. Li, P. Xu, Z. Ren, B. Zhang, Y. Du, X. Han, N.H. Mack, N.-L. Wang, ACS Appl. Mater. Interfaces 5 (2013) 49–54.
[18] J.-H. Hong, Y.-K. Hwang, J.-Y. Hong, H.-J. Kim, S.-J. Kim, Y.S. Wonc, S. Huh, Chem. Commun. 47 (2011) 6963–6965.
[19] H.-S. Shin, J.-Y. Hong, S. Huh, ACS Appl. Mater. Interfaces 5 (2013) 1429–1435.
[20] R. Baigorri, J.M. García-Mina, R.F. Aroca, R.A. Alvarez-Puebla, Chem. Mater. 20 (2008) 1516–1521.

[21] S. Goy-López, J. Juárez, A. Cambón, J. Botana, M. Pereiro, D. Baldomir, P. Taboada, V. Mosquera, J. Mater. Chem. 20 (2010) 6808–6814.
[22] G. Lin, W. Lu, W. Cui, L. Jiang, Cryst. Growth Des. 10 (2010) 1118–1123.
[23] D.A. Walker, K.P. Browne, B. Kowalczyk, B.A. Grzybowski, Angew. Chem. Int. Ed. 49 (2010) 6760–6763.
[24] H. Liu, Q. Yang, CrystEngComm 13 (2011) 2281–2288.
[25] B. Cao, B. Liu, J. Yang, CrystEngComm 15 (2013) 5735–5738.
[26] J.E. Millstone, S. Park, K.L. Shuford, L. Qin, G.C. Schatz, C.A. Mirkin, J. Am. Chem. Soc. 127 (2005) 5312–5313.
[27] C.S. Ah, Y.J. Yun, H.J. Park, W.-J. Kim, D.H. Ha, W.S. Yun, Chem. Mater. 17 (2005) 5558–5561.
[28] S.R. Beeram, F.P. Zamborini, ACS Nano 4 (2010) 3633–3646.
[29] X. Fan, Z.R. Guo, J.M. Hong, Y. Zhang, J.N. Zhang, N. Gu, Nanotechnology 21 (2010) 105602.
[30] Z. Sun, X. Chen, L. Wang, G. Zhang, B. Jing, Eng. Aspects 326 (2008) 23–28.
[31] H.M. Chen, R.-S. Liu, D.P. Tsai, Cryst. Growth Des. 9 (2009) 2079–2087.
[32] H.-C. Chu, C.-H. Kuo, M.H. Huang, Inorg. Chem. 45 (2006) 808–813.
[33] W.-L. Huang, C.-H. Chen, M.H. Huang, J. Phys. Chem. C 111 (2007) 2533–2538.
[34] S. Hong, K.L. Shuford, S. Park, Chem. Mater. 23 (2011) 2011–2013.
[35] P.J. Straney, C.M. Andolina, J.E. Millstone, Langmuir 29 (2013) 4396–4403.
[36] C. Kan, X. Zhu, G. Wang, J. Phys. Chem. B 110 (2006) 4651–4656.
[37] J.-H. Lee, K. Kamada, N. Enomoto, J. Hojo, Cryst. Growth Des. 8 (2008) 2638–2645.
[38] A.A. Umar, M. Oyama, Cryst. Growth Des. 6 (2006) 818–821.
[39] Y. Xiong, I. Washio, J. Chen, H. Cai, Z.-Y. Li, Y. Xia, Langmuir 22 (2006) 8563–8570.
[40] G. Zhan, L. Ke, Q. Li, J. Huang, D. Hua, A.-R. Ibrahim, D. Sun, Ind. Eng. Chem. Res. 51 (2012) 15753–15762.
[41] B. Pelaz, V. Grazu, A. Ibarra, C. Magen, P. Del Pino, J.M. De La Fuente, Langmuir 28 (2012) 8965–8970.
[42] W.-H. Lin, Y.-J. Hsu, in: 2010 International Conference on Biology, Environmental, and Chemistry, IPCBEE, vol. 1, 2001, pp. 289–292.
[43] T.K. Sau, C.J. Murphy, J. Am. Chem. Soc. 126 (2004) 8648–8649.
[44] V. Germain, J. Li, D. Ingert, Z.L. Wang, M.P. Pileni, J. Phys. Chem. B 107 (2003) 8717–8720.
[45] J. Zeng, J. Tao, W. Li, J. Grant, P. Wang, Y. Zhu, Y. Xia, Chem. Asian J. 6 (2011) 376–379.
[46] J.D. Verhoeven, Fundamentals of Physical Metallurgy, John-Wiley & Sons, 1975.
[47] Y. Xiong, Y. Xia, Adv. Mater. 19 (2007) 3385–3391.
[48] C. Lofton, W. Sigmund, Adv. Funct. Mater. 15 (2005) 1197–1208.
[49] P. Jiang, J.-J. Zhou, R. Li, Y. Gao, T.-L. Sun, X.-W. Zhao, Y.-J. Xiang, S.-S. Xie, J. Nanoparticle Res. 8 (2006) 927–934.
[50] C. Wang, C. Kan, J. Zhu, X. Zeng, X. Wang, H. Li, D. Shi, J. Nanomater. (2010) 969030.
[51] F. Kim, S. Connor, H. Song, T. Kuykendall, P. Yang, Angew. Chem. Int. Ed. 43 (2004) 3673–3677.
[52] B.J. Wiley, S.H. Im, Z.-Y. Li, J. McLellan, A. Siekkinen, Y. Xia, J. Phys. Chem. B 110 (2006) 15666–15675.
[53] J.E. Millstone, G.S. Métraux, C.A. Mirkin, Adv. Funct. Mater. 16 (2006) 1209–1214.
[54] G. Laurent, N. Félidj, J. Grand, J. Aubard, G. Lévi, Phys. Rev. B 73 (2006) 245417.
[55] R.R. Naujok, R.V. Duevel, R.M. Corn, Langmuir 9 (1993) 1771–1774.
[56] N. Félidj, J. Aubard, G. Lévi, Phys. Rev. B 65 (2002) 075419.
[57] N.E. Sánchez, J. Salafranca, A. Callejas, Á. Millera, R. Bilbao, M.U. Alzueta, Fuel 107 (2013) 246–253.
[58] L. Guerrini, J.V. Garcia-Ramos, C. Domingo, S. Sanchez-Cortes, Anal. Chem. 81 (2009) 1418–1425.
[59] L. Guerrini, A.E. Aliaga, J. Cárcamo, J.S. Gómez-Jeria, S. Sanchez-Cortes, M.M. Campos-Vallette, J.V. García-Ramos, Anal. Chim. Acta 624 (2008) 286–293.
[60] P. Leyton, S. Sanchez-Cortes, J.V. Garcia-Ramos, C. Domingo, M. Campos-Vallette, C. Saitz, R.E. Clavijo, J. Phys. Chem. B 108 (2004) 17484–17490.
[61] J. Vial, A. Jardy, Anal. Chem. 71 (1999) 2672–2677.
[62] L. Guerrini, J.V. Garcia-Ramos, C. Domingo, S. Sanchez-Cortes, Anal. Chem. 81 (2009) 953–960.
[63] L. Guerrini, J.V. Garcia-Ramos, C. Domingo, S. Sanchez-Cortes, Phys. Chem. Chem. Phys. 11 (2009) 1787–1793.